JOURNAL OF GUIDANCE, CONTROL, AND DYNAMICS
Vol. 15, No. 3, May-June 1992

Nonlinear Control Law with Application to High Angle-of-Attack Flight

Daniel J. Bugajski* and Dale F. Enns†
Honeywell Systems and Research Center, Minneapolis, Minnesota 55418

This paper proposes a general structure for aircraft control at whose core are several blocks of dynamic inversion of the controlled system. This control law is then applied to a nonlinear model of the high angle-of-attack research vehicle (HARV). The control law itself uses the complete nonlinear aerodata base and has no restrictions on the manner in which the control inputs enter the dynamic equations. An algorithm that handles surface limiting while ensuring a solution to the moment equation inverse is incorporated into the control law. The performance of the control law is demonstrated via simulation of a selected supermaneuver.

Introduction

FIGHTER aircraft capable of maneuvering at extremely high angles of attack without fear of loss of control will have significant advantages over opponents without such capability.[1] Advanced control laws will be required to achieve this added capability. Control laws for high angle-of-attack maneuvering will be more nonlinear than conventional flight control laws. The nonlinearities are a consequence of nonlinear aerodynamics and nonlinear inertial couplings in this flight regime.

This paper will present nonlinear control laws intended for flight in this regime. The control laws are based on inverting the dynamic and kinematic equations of motion. That is, forces and moments corresponding to undesired aerodynamic, gravitational, or inertial contributions are modeled as functions of measured state variables. Opposing forces and moments are then commanded to negate the undesired contributions followed by application of desired forces and moments needed to accomplish the maneuver. This concept for nonlinear aircraft flight control has received a great deal of attention in recent years. Nonlinear decoupling theory has been applied to aircraft flight control,[2-4] as well as linearizing transformations of states and controls.[5,6] Various flight-test evaluations have also provided some experience with these techniques.[7-10]

Direct application of the general theory[2,3,5,6] to aircraft flight control is not possible because the usual four aircraft controls (thrust, aileron, rudder, and elevator) are not sufficient to decouple and control six degrees of freedom. Successful applications have been made to aircraft flight control, however, with some approximation or simplification. A common approximation is to neglect the aerodynamic lift and side force contributions of the control surfaces to the equations of motion. Another approach is called partial dynamic inversion[11] and has also been applied to highly nonlinear aircraft flight control.[12]

In this paper, the roll, pitch, and yaw moments are controlled with the effective aileron, elevator, and rudder. In some cases, the effective control surface is some combination of more than one surface and/or thrust vectoring control. Desired moments are calculated based on the rigid-body moment equation of motion to control roll, pitch, and yaw angular rates. Other researchers have used this approach in nonlinear aircraft flight control.[13,14]

The body attitudes relative to the airflow are then controlled with the three angular rate commands. Desired angular rates are calculated based on kinematic equations to control bank angle, sideslip angle, and angle of attack. This concept has been discussed with respect to slow and fast variables in the context of singular perturbation theory.[15,16]

The aircraft velocity vector is controlled with thrust and aircraft attitude commands. Desired thrust and attitude of the aircraft relative to the airflow are calculated based on the point mass equations of motion to control velocity, heading, and flight-path angle. The use of thrust and vehicle attitude relative to airflow to control the velocity vector has been recognized in the literature.[4,13,17-21]

In this paper, there is no restriction put on the manner in which the control inputs enter the equations of motion. Specifically, they do not enter additively or additive with nonsingular multipliers. This generality necessitates non-closed-form solutions for the inverse such as Newton-Raphson iterative techniques similar to those used in Ref. 22.

Control surface saturations pose serious limitations to rapid maneuvering. This paper discusses a method for accounting for control surface saturations. This approach scales the desired rates of change of body angular rates just enough to put surfaces on their limits. This amounts to real-time decreases in bandwidth.

An ideal testbed for this nonlinear control concept is the high angle-of-attack research vehicle (HARV). The HARV is the flight-test vehicle for NASA's research program to study the issues associated with flight at high angles of attack. The data base for this aircraft provided for application of the dynamic inversion control laws developed in this paper.

Models

This section details the aircraft model used in this study. There were no dynamic sensor models, i.e., the transfer function for each of the sensors is unity. Similarly, no actuator dynamics were used for the majority of the study. The effect of actuator dynamics was studied on a sample supermaneuver by including both 30 and 100 rad/s first-order lags to model dominant surface actuator effects. Both showed negligible performance degradation.

The aircraft 6 degree-of-freedom equations of motion are given in the following 12 first-order, nonlinear differential equations. The states chosen are body roll rate p, body pitch rate q, body yaw rate r, velocity roll angle μ, angle of attack

Received June 6, 1990; presented as Paper 90-3407 at the AIAA Guidance, Navigation, and Control Conference, Portland, OR, Aug. 20-22, 1990; revision received July 1, 1991; accepted for publication July 19, 1991.

*Principal Research Engineer, 3660 Technology Drive. Member AIAA.

†Senior Research Fellow, 3660 Technology Drive; also Adjunct Associate Professor, University of Minnesota, Department of Aerospace Engineering and Mechanics, Minneapolis, MN 55455. Member AIAA.

α, sideslip angle β, velocity V, heading angle χ, flight-path angle γ, a horizontal displacement with respect to an inertial reference frame, e.g., North x, a similar displacement in an orthogonal direction, e.g., East y, and altitude h (formal definitions for μ and χ can be found in Ref. 23):

$$\begin{bmatrix}\dot{p}\\ \dot{q}\\ \dot{r}\end{bmatrix} = I^{-1}\left\{ -\begin{bmatrix}0 & -r & q\\ r & 0 & -p\\ -q & p & 0\end{bmatrix} I \begin{bmatrix}p\\ q\\ r\end{bmatrix} + \begin{bmatrix}l_A\\ M_A\\ N_A\end{bmatrix} + \begin{bmatrix}0\\ M_T\\ N_T\end{bmatrix}\right\} \tag{1-3}$$

$$\dot{\mu} = \frac{\cos(\alpha)}{\cos(\beta)}p + \frac{\sin(\alpha)}{\cos(\beta)}r + \tan(\beta)\cos(\mu)\dot{\gamma} + [\sin(\gamma) + \tan(\beta)\sin(\mu)\cos(\gamma)]\dot{\chi} \tag{4}$$

$$\dot{\alpha} = -\cos(\alpha)\tan(\beta)p + q - \sin(\alpha)\tan(\beta)r - \frac{\cos(\mu)}{\cos(\beta)}\dot{\gamma} - \sin(\mu)\frac{\cos(\gamma)}{\cos(\beta)}\dot{\chi} \tag{5}$$

$$\dot{\beta} = \sin(\alpha)p - \cos(\alpha)r - \sin(\mu)\dot{\gamma} + \cos(\mu)\cos(\gamma)\dot{\chi} \tag{6}$$

$$\dot{V} = \frac{1}{m}\left[-\cos(\beta)D + \sin(\beta)Y \right. \tag{7}$$

$$\dot{\chi} = \frac{1}{mV\cos(\gamma)}[\sin(\beta)\cos(\mu)D + \sin(\mu)L + \cos(\beta)\cos(\mu)Y] + \frac{1}{mV\cos(\gamma)}F_{\chi T} \tag{8}$$

$$\dot{\gamma} = \frac{-\sin(\beta)\sin(\mu)D}{mV} + \frac{\cos(\mu)}{mV}L - \frac{\cos(\beta)\sin(\mu)}{mV}Y - \frac{\cos(\gamma)}{V}g + \frac{1}{mV}F_{\gamma T} \tag{9}$$

$$\dot{x} = \cos(\gamma)\cos(\chi)V \tag{10}$$

$$\dot{y} = \cos(\gamma)\sin(\chi)V \tag{11}$$

$$\dot{h} = \sin(\gamma)V \tag{12}$$

where l_A, M_A, N_A, D, Y, and L are the aerodynamic contributions to roll, pitch, yaw, drag, side force, and lift, respectively, which are generated by interpolation through a nonlinear data base. Variables subscripted with a T are appropriate contributions from thrust, including thrust vectoring capability; m is the aircraft mass; g is the gravitational constant; and I is the moment of inertia matrix.

The aerodynamic forces and moments were obtained through interpolation of a complete set of aerodynamic coefficient and derivative tables for the HARV. The data base provided for α ranging between -12 and 90 deg, β ranging between -20 and 20 deg, Mach number ranging between 0.2 and 2.0, and h to 60,000 ft.

The model provided for 10 control surfaces; left and right leading-edge flaps, left and right trailing-edge flaps, left and right ailerons, left and right stabilators, and left and right rudders. An α/Mach schedule for the leading- and trailing-edge flaps was implicitly incorporated into part of the data base, and thus the schedule was used with the remainder of the data base to insure smooth interpolations between parts of the data. For this reason, the leading- and trailing-edge schedules are implicit in the control laws developed here.

Control Laws

In this section we develop the control laws used in this study. We will show how the dynamic inversion parts of the control law fit into a classical control-type structure. As the term "dynamic inversion" implies, we will be inverting (in some sense) the dynamics of our system. Thus it will be helpful to review the airplane dynamic model of the previous section in a somewhat different form. A general form of our aircraft model can be written as follows:

$$\dot{x} = F(x,u) \tag{13}$$

Specifically, let

$$x = \begin{bmatrix}x_1\\ x_2\\ x_3\\ x_4\end{bmatrix} = \begin{bmatrix}(p,q,r)^T\\ (\mu,\alpha,\beta)^T\\ (V,\chi,\gamma)^T\\ (x,y,h)^T\end{bmatrix}$$

$$u = \begin{bmatrix}\delta\\ T\\ \delta_{\text{flaps}}\end{bmatrix} = \begin{bmatrix}(\delta_a,\delta_e,\delta_r)^T\\ T\\ \delta_{\text{flaps}}\end{bmatrix}$$

where δ_a, δ_e, and δ_r represent differential aileron deflections, symmetric elevator deflections, and symmetric rudder deflections.

Breaking up Eq. (13) into four vector differential equations, we get

Body rate equations:

$$\dot{x}_1 = F_1(x_1,x_2,x_3,x_4,\delta,T,\delta_{\text{flaps}}) \tag{14}$$

Attitude equations:

$$\dot{x}_2 = F_2(x_1,x_2,x_3,x_4,\delta,T,\delta_{\text{flaps}}) \tag{15}$$

Velocity equations:

$$\dot{x}_3 = F_3(x_1,x_2,x_3,x_4,\delta,T,\delta_{\text{flaps}}) \tag{16}$$

Position equations:

$$\dot{x}_4 = F_4(x_3) \tag{17}$$

These equations are explicit but require table lookups to determine the aerodynamic contributions. With this particular selection of state variables, the aircraft dynamics essentially line up as shown in Fig. 1.

With the earlier functions (which represent our model dynamics) in mind, we present the functions that represent the inverse dynamics:

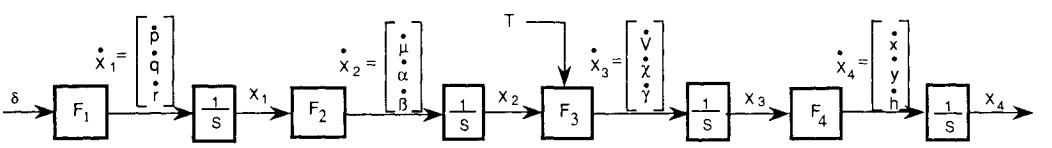

Fig. 1 Simplified block diagram of aircraft dynamics.

Body rate control:

$$\delta = K_1(x_1,x_2,x_3,x_4,T,\delta_{\text{flaps}},\dot{x}_1) \tag{18}$$

Attitude control:

$$x_1 = K_2(x_2,x_3,x_4,\delta,T,\delta_{\text{flaps}},\dot{x}_2) \tag{19}$$

Velocity control:

$$(x_2,T) = K_3(x_1,x_3,x_4,\delta,\delta_{\text{flaps}},\dot{x}_3) \tag{20}$$

Position control:

$$x_3 = K_4(\dot{x}_4) \tag{21}$$

Note that these functions are essentially rewritten versions of Eqs. (14–17). Equations (18–20) each require an iteration because the right-hand sides of the equations (namely, the $\dot{x}_i$) depend on the variables on the left-hand sides through the nonlinear data base. These iterations are set up so that the variables on the left-hand sides of the equalities are chosen to achieve a set of desired $\dot{x}_i$. Note that Eq. (20) has four free variables available to achieve the three desired values in $\dot{x}_3$. We will fix one of the free variables to use this extra degree of freedom. Then each of these iterations has three free variables and three constraints, and we use a first-order Newton-Raphson search starting from the previous solution to get a solution for the current time. Note that Eq. (21) can be solved explicitly.

To illustrate how the dynamic inversion control works, suppose first that we are able to select a set of desired angular accelerations, $\dot{p}$, $\dot{q}$, $\dot{r}$ ($= \dot{x}_1$), that will allow us to complete some maneuver. Then solving the body rate stabilization equations (18) with this desired $\dot{x}_1$ generates a set of surface deflections. The surface deflections enter the aircraft model through the function F_1. If $K_1 \approx F_1^{-1}$, then the surface deflection commands, out of K_1 and into F_1, will produce the $\dot{x}_1$ that we desired. Now that we have a piece of the control law that will force the aircraft to generate the desired angular accelerations, we need to pick the desired angular accelerations. We do this with the classical type of feedback structure shown in Fig. 2. Using this structure, there is merely an integration between the desired angular accelerations and the angular rates. The diagonal gain matrix B_1 sets the bandwidth for the angular rate loops. Thus, below the bandwidth B_1, the state x_1 will track the commanded value of x_1.

At this point, we are left with generating the commands for the body rates. Since the function K_2 [Eq. (19)] is set up to produce angular rates, it will be used to generate the commands to the body rate loops. To solve Eq. (19), we need to identify a set of desired attitude rates ($\dot{x}_2 = [\dot{\mu},\dot{\alpha},\dot{\beta}]$). We do this with a feedback structure analogous to the body rate loop closure as shown in Fig. 3. Here B_2 sets the bandwidth for these loops.

Analogously, we add a guidance loop based on the dynamic inversion function K_3 to control the velocity vector. This will aid in the simulation of known supermaneuvers that are defined in terms of V, χ, γ ($= x_3$) time histories. Recall that the

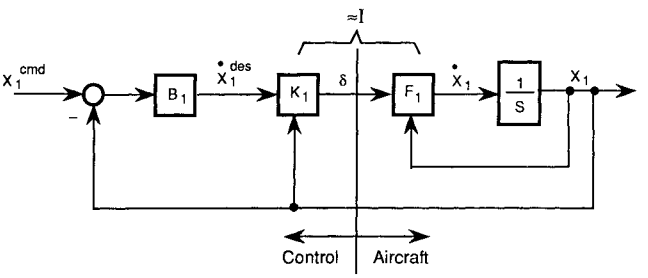

Fig. 2 Body rate feedback loop.

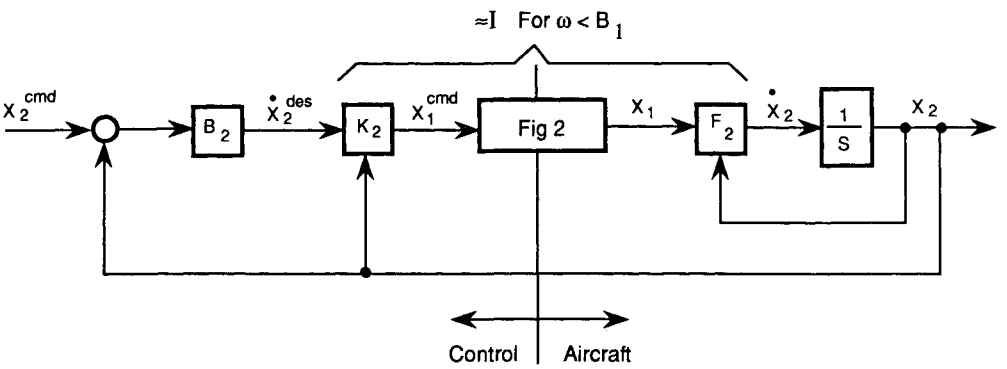

Fig. 3 Body attitude feedback loop.

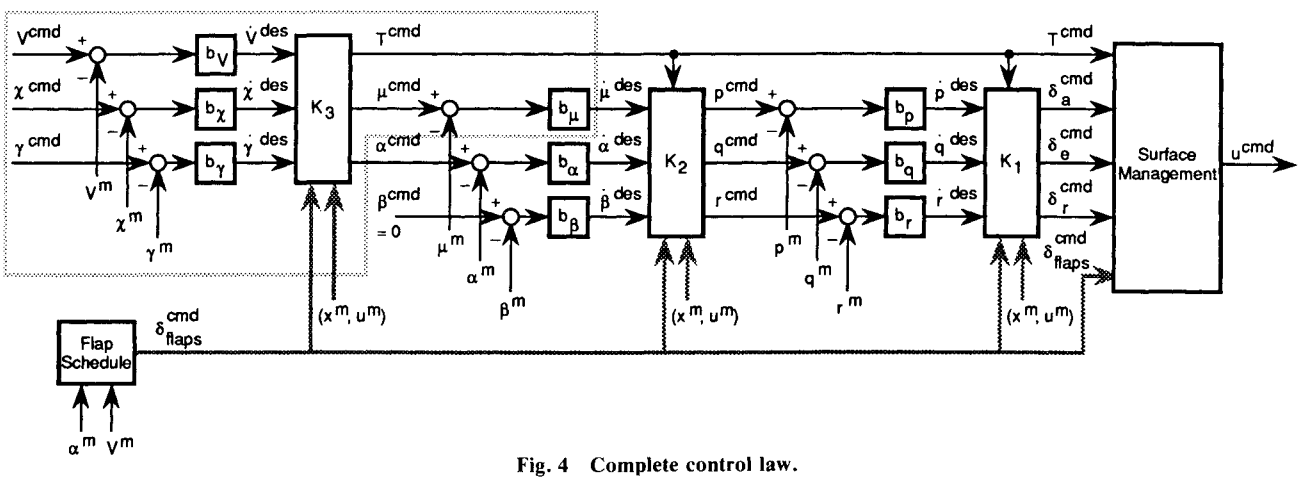

Fig. 4 Complete control law.

function K_3 has four free variables and three equations. Since one of the free variables is sideslip angle, and since we prefer coordinated flight, we fix the sideslip command to be zero. (Note that we could have added a navigation-type loop by using the dynamic inversion function K_4, but that is not our interest here.)

Finally we arrive at the control law block diagram shown in Fig. 4. In the figure, the dashed line encloses what are usually termed "outer loop" control functions. Our purpose in adding them is only to aid in the simulation of maneuvers. The remainder of the control law has a classical inner loop control law structure in that the airplane is stabilized with angular rate feedback, and its attitude is controlled with somewhat slower loops. In addition to their classical structure, these loops rely on a couple blocks of dynamic inversion.

Surface Command Limiting

In this section we describe the algorithm used to limit the surface deflection ($\delta = [\delta_a, \delta_e, \delta_r]$) commands to the aircraft. Because there are limits on actuator deflections, there will be implied, state-dependent limits on the resulting angular accelerations. Take, for example, a simplified linear model for the roll dynamics: $\dot{p} = L_p p + L_\delta \delta_a$. Then for any roll rate p there is a maximum roll acceleration $\dot{p}^{\max}$ that corresponds to the maximum surface deflection $\delta_a^{\max}$. In general, this type of nonlinearity might be lumped in with the nonlinearities included in our F_1 function. Recall that the K_1 function essentially inverts F_1 by calculating a set of surface deflections given a desired set of angular accelerations. But because saturations are noninvertible nonlinearities, the previously described rate loop computations (especially the evaluation of the K_1 function) are not well defined. It seems, though, that a way of dealing with these limits would naturally be incorporated into the rate loop computations. Our method of dealing with saturations will be to reduce the bandwidth of the rate loops such that 1) the (scaled) $\dot{x}_1^{\text{des}}$ is achieved and 2) a surface is on its limit.

We write the Newton-Raphson iteration for the evaluation of the K_1 function as follows:

$$\delta(n+1) = \left[\left.\frac{\partial F_1(x^o,u)}{\partial \delta}\right|_{u=u(n)}\right]^{-1} \{\dot{x}_1^{\text{des}} - F_1[x^o,u,(n)]\} + \delta(n) \tag{22}$$

where x^o indicates the current state, the superscript "des" indicates a desired value, and the index n is the Newton-Raphson step counter. Note that the right-hand side of Eq. (22) includes a term due to the desired angular accelerations and a term due to the current angular accelerations. Further, the only term specified by the designer is $\dot{x}_1^{\text{des}}$, which we have currently defined to be $B_1(x_1^{cmd} - x_1)$. All other terms on the right-hand side of this equation are known or easily computed.

The previous iteration works fine until the choice of desired angular accelerations is such that no allowable deflections will achieve it. This can be depicted with the two-dimensional vector representation shown in Fig. 5. The left diagram shows the maximum deflection boundary. The right diagram shows two possible mappings (we have shown mappings into rectangles for simplicity) of the deflection boundary into the angular acceleration space giving two possible acceleration boundaries. The larger rectangle corresponds to a high dynamic pressure ($\bar{q}$) flight condition (i.e., surfaces are more effective), and the smaller rectangle corresponds to a low dynamic pressure flight condition. Also drawn on this figure are vectors representing the desired angular acceleration and the angular acceleration due to the existing state. The controls must make up the difference to achieve the desired angular acceleration. But since the desired angular acceleration lies outside of the achievable limits, there is no solution. Our experience has shown that scaling back the $\dot{x}_1^{\text{des}}$ vector (i.e., retaining the direction but decreasing the magnitude) such that the resultant scaled vector sum lies on the acceleration boundary yields the best results.

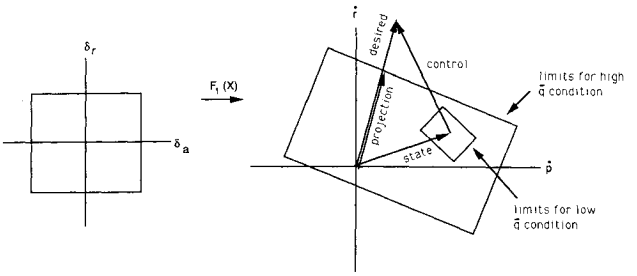

Fig. 5 Two-dimensional depiction of limiting algorithm.

While this solution only holds for cases like the high dynamic pressure case, it has the following intuitive appeal: actuator saturations tend to imply that the closed-loop system gain/bandwidth is too high; conversely, if it is known that actuators are going to saturate, perhaps the bandwidth should be reduced. Indeed, this is what the algorithm does. Since $\dot{x}_1^{\text{des}} = B_1 x_1^{\text{error}}$, scaling $\dot{x}_1^{\text{des}}$ is equivalent to scaling B_1, the bandwidth of the x_1 loops.

Note that for the low dynamic pressure case, the algorithm described previously will fail since there is no way to scale back along the desired acceleration vector until valid accelerations are achieved. In such an instance, the flight is uncontrolled and will result in instability unless the aircraft passes through a controllable part of the state-space and control is reacquired. It should also be noted that this logic has been incorporated into the x_1 loops only. Limiting for the other loops has not been implemented.

Results

In this section we show, by way of simulation of a supermaneuver, the performance of the control strategy detailed earlier. (While we refer to this maneuver as a "supermaneuver," it should be noted that the angles of attack that are achieved do not go that deeply into the poststall region.) The supermaneuver is based on the time history information included in Ref. 24 and defined by V, χ, and γ. The maneuver is time optimal and designed to reverse the direction of both the velocity vector and the body x axis. The maneuver begins at 100 m/s and finishes flying straight and level at 62 m/s.

We have chosen the following bandwidths for the control loops: $B_1 = 5$ rad/s, $B_2 = 1$ rad/s, and $B_3 = 0.2$ rad/s. Bandwidths for velocity and attitude loops used here are considered low compared to values of 1 rad/s for flight-path angle and 2-3 rad/s for angle of attack that would be more appropriate for conventional maneuvers. It may be possible to obtain these higher bandwidths during supermaneuvers with the addition of thrust vectoring control, but this was beyond the scope of this study.

Figure 6 contains the simulation results for the supermaneuver. In all cases where two traces are on the same grid, the solid line corresponds to the commanded value of the signal, whereas the dashed line indicates the actual value. Parts a) through c) show V, χ, and γ ($= x_3$). They have tracking consistent with a 5-s time constant. Parts d) through f) show μ, α, and β ($= x_2$). Here again we see good tracking, consistent with a 1-s time constant. Peak angle of attack during the transient is about 46 deg, and it finishes up at about 39 deg. Recall the sideslip command is always zero, and we get a peak sideslip angle of about 1 deg. Parts g) through i) show p, q, and r ($= x_1$). With the exception of the intervals of rudder saturation (when the limiting logic forces a bandwidth reduction), these show good tracking and no extraordinary magnitudes. Parts j) through l) show the effective surfaces δ_a, δ_e, and δ_r ($= \delta$). Parts m) through o) show the thrust, lateral acceleration, and normal acceleration. Lateral acceleration

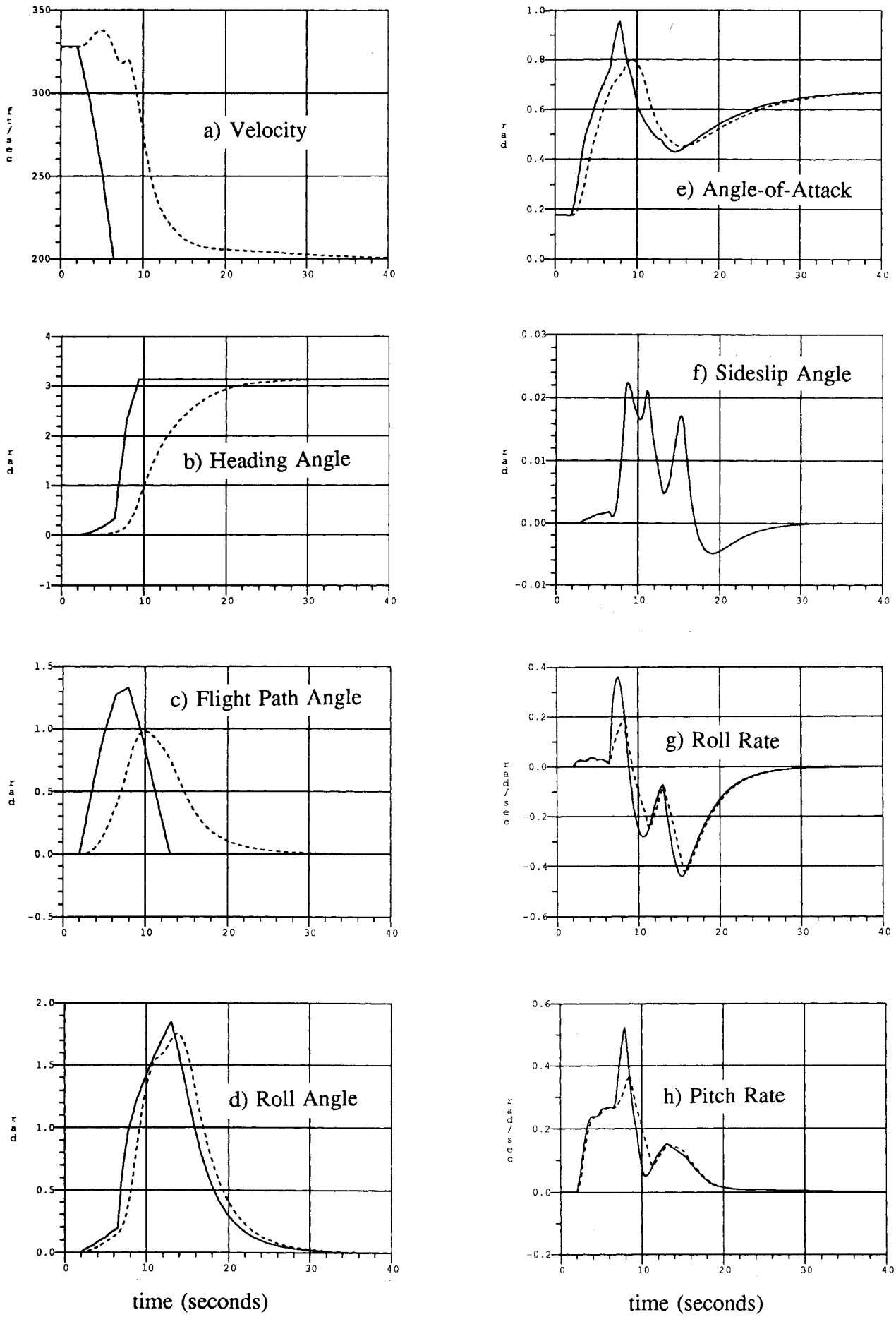

Fig. 6 HARV simulation results.

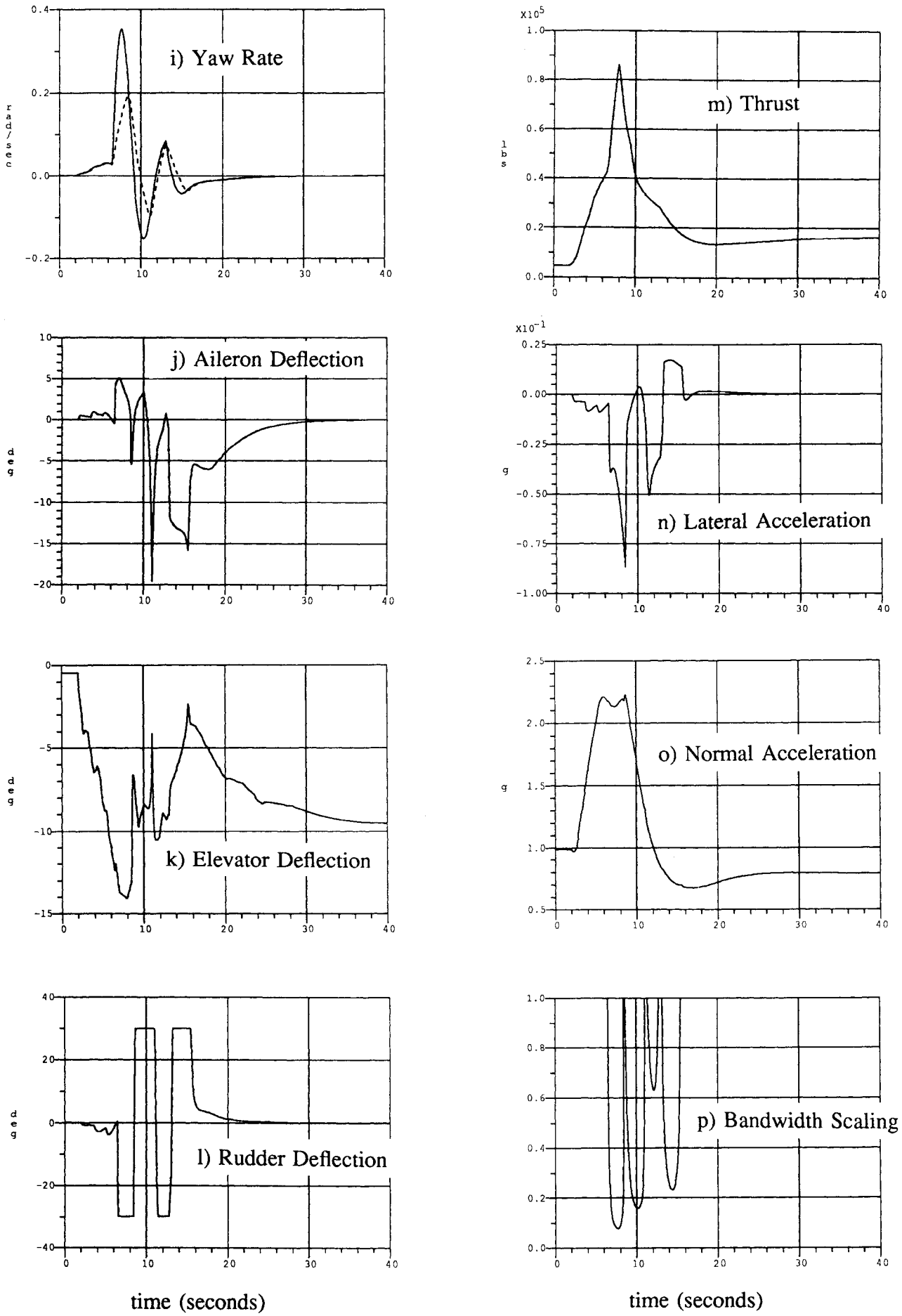

Fig. 6 (continued) HARV simulation results.

peaks at 0.08 g and is small (<0.05 g) everywhere else. Normal acceleration peaks at about 2.2 g. Clearly the thrust response is unrealistic, as no limits were incorporated into this part of the control law. Finally, part p) shows the scale factor used to reduce the rate loop bandwidth. At the worst case, the bandwidth was reduced to 10% of its nominal value. Note that at the time of peak thrust, there are noticeable irregularities in some of the other traces as well. This is best explained by a time mismatch problem between the variables commanded by the velocity loop. The velocity loop commands thrust and angle of attack, but only the thrust responds instantaneously (since there are no actuator dynamics), angle of attack does not (since it is slowed by its own control loop). Overall the control system performed very well, providing precise tracking in all three axes throughout this highly coupled maneuver.

Simulation of more demanding supermaneuvers, those requiring turning at higher angles of attack or slower speeds, shows that the lack of rudder authority results in instability. This was expected and would be overcome by the addition of thrust vectoring capability or nose strakes.[16,25] Models for these modifications were not included due to resource limitations.

Conclusions

We have defined a general structure for a set of advanced nonlinear control laws. While these control laws have a classical flavor, the core pieces are based on the technique of dynamic inversion. We have implemented these control laws with a model of the HARV. The control laws, as well as the aircraft model, use a full nonlinear aerodata base. We have also implemented an algorithm to handle appropriate surface limiting while insuring a solution to the iterative solutions inherent in the dynamic inversion methodology. Via simulation we have shown that the control laws exhibit excellent tracking performance.

References

[1]Schefter, J., "X-31, How They're Inventing a Radical New Way to Fly," *Popular Science Magazine,* Vol. 234, No. 2, 1989, pp. 58–64.

[2]Singh, S. N., and Rugh, W. J., "Decoupling in a Class of Nonlinear Systems by State Variable Feedback," *Journal of Dynamic Systems, Measurement, and Control,* ASME Transactions Series G, Vol. 94, No. 12, 1972, pp. 323–329.

[3]Asseo, S. J., "Decoupling of a Class of Nonlinear Systems and Its Applications to an Aircraft Control Problem," *Journal of Aircraft,* Vol. 10, No. 12, 1973, pp. 739–747.

[4]Singh, S. N., and Schy, A. A., "Nonlinear Decoupled Control Synthesis for Maneuvering Aircraft," *Proceedings of the 1978 IEEE Conference on Decision and Control,* IEEE, Piscataway, NJ, Jan. 1979, pp. 360–370.

[5]Meyer, G., "The Design of Exact Nonlinear Model Followers," *Proceedings of the 1981 Joint Automatic Control Conference,* IEEE, Paper No. FA-3A, Piscataway, NJ, June 1981.

[6]Meyer, G., Su, R., and Hunt, L. R., "Applications of Nonlinear Transformations to Automatic Flight Control," *Automatica,* Vol. 20, No. 1, 1984, pp. 103–107.

[7]Cicolani, L. S., Sridhar, B., and Meyer, G., "Configuration Management and Automatic Control of an Augmentor Wing Aircraft with Vectored Thrust," NASA TP 1222, March 1979.

[8]Franklin, J. A., Hynes, C. S., Hardy, G. H., Martin, J. L., and Innis, R. C., "Flight Evaluation of Augmented Controls for Approach and Landing of Powered-Lift-Aircraft," *Journal of Guidance, Control, and Dynamics,* Vol. 9, No. 5, 1986, pp. 555–565.

[9]Franklin, J. A., Stortz, M. W., Gerdes, R. M., Hardy, G. H., Martin, J. L., and Engelland, S. A., "Simulation Evaluation of Transition and Hover Flying Qualities of the E-7A STOVL Aircraft," NASA TM 101015, Aug. 1988.

[10]Franklin, J. A., Stortz, M. W., Engelland, S. A., Hardy, G. H., Martin, J. L., and Gerdes, R. M., "Simulation Evaluation of Transition and Hover Flying Qualities of a Mixed-Flow Remote-Lift STOVL Aircraft," NASA TM 102274, Feb. 1990.

[11]Elgersma, M. R., "Control of Nonlinear Systems Using Partial Dynamic Inversion," Ph.D. Dissertation, Control Sciences Dept., Univ. of Minnesota, Minneapolis, MN, 1988.

[12]Elgersma, M. R., Morton, B. M., Harvey, C. A., and Hines, G., "Nonlinear Flying Quality Parameters Based on Dynamic Inversion," Final Report to Flight Dynamics Lab., AFWAL-TR-87-3079, Wright-Patterson AFB, OH, Oct. 1987.

[13]Lane, S. H., and Stengel, R. F., "Flight Control Design Using Nonlinear Inverse Dynamics," *Proceedings of the 1986 American Control Conference,* IEEE, Piscataway, NJ, June 1986, pp. 587–596.

[14]Morton, B. M., Elgersma, M. R., Enns, D. F., and Suchomel, C., "Application of Dynamic Inversion to Improve Oblique Wing Aircraft Flying Qualities," National Aerospace Electronics Conference, IEEE, Piscataway, NJ, May 1986.

[15]Menon, P. K. A., Badgett, M. E., Walker, R. A., and Duke, E. L., "Nonlinear Flight Test Trajectory Controllers for Aircraft," *Journal of Guidance, Control, and Dynamics,* Vol. 10, No. 1., 1987, pp. 67–72.

[16]Snell, S. A., Enns, D. F., and Garrard, W. L., "Nonlinear Inversion Flight Control for a Supermaneuverable Aircraft," *Proceedings of the 1990 AIAA Guidance, Navigation, and Control Conference,* Washington, DC, Aug. 1990, pp. 808–825.

[17]Kato, O., and Sugiura, I., "An Interpretation of Airplane General Motion and Control as Inverse Problem," *Journal of Guidance, Control, and Dynamics,* Vol. 9, No. 2, 1986, pp. 198–204.

[18]Neumark, S., "Problems of Longitudinal Stability Below Minimum Drag Speed, and Theory of Stability Under Constraint," Aeronautical Research Council R&M No. 2983, London, July 1953.

[19]Ashkenas, I. L., and Craig, S. J., "Multiloop Piloting Aspects of Longitudinal Approach Path Control," International Council of the Aeronautical Sciences, Paper No. 72-46, Amsterdam, Aug. 1972.

[20]Franklin, J. A., and Innis, R. C., "Flightpath and Airspeed Control During Landing Approach for Powered-Lift Aircraft," NASA TN D-7791, Oct. 1974.

[21]Craig, S. J., Ashkenas, I. L., and Heffley, R. K., "Pilot Background and Vehicle Parameters Governing Control Technique in STOL Approach Simulations," Federal Aviation Administration, FAA-RD-72-69, Washington, DC, June 1972.

[22]Smith, G. A., and Meyer, G., "Aircraft Automatic Flight Control System with Model Inversion," *Journal of Guidance, Control, and Dynamics,* Vol. 10, No. 3, 1987, pp. 269–275.

[23]Miele, A., *Flight Mechanics, Theory of Flight Paths,* Vol. 1, Addison-Wesley, Reading, MA, 1962.

[24]Well, K. H., Faber, B., and Berger, E., "Optimale Taktische Flugmanöver für ein Kampfflugzeug der 90er Jahre," Interner Breicht A-552-79/6, DFVLR, Oberpfaffenhoffen, Germany, 1979.

[25]Ashley, H., and Clarke, L., "On the Feasibility of Low Speed Fighter Maneuvers Involving Extreme Angles of Attack," Stanford Univ. Technical Document SUDAAR 563, Stanford, CA, July 1987.